Chinese Chemical Letters 31 (2020) 3107–3112

Contents lists available at ScienceDirect

Chinese Chemical Letters

journal homepage: www.elsevier.com/locate/cclet

Communication

# *In situ* construction of ligand nano-network to integrin $\alpha_v\beta_3$ for angiogenesis inhibition

Ziming Chen[a,b], Kuo Zhang[b], Jiaqi Fan[b], Yu Fan[b], Chao Yang[b], Wen Tian[b], Yuan Li[b], Wenliang Li[a], Jingping Zhang[a], Hao Wang[b], Lei Wang[b,*]

[a] *Faculty of Chemistry, Northeast Normal University, Changchun 130024, China*
[b] *CAS Center for Excellence in Nanoscience, CAS Key Laboratory for Biomedical Effects of Nanomaterials and Nanosafety, National Center for Nanoscience and Technology (NCNST), Beijing 100190, China*

ARTICLE INFO

*Article history:*
Received 13 February 2020
Received in revised form 2 April 2020
Accepted 4 April 2020
Available online 20 April 2020

*Keywords:*
Self-assembly
Integrin $\alpha_v\beta_3$
Peptide
Anti-angiogenesis
Tumor

ABSTRACT

Angiogenesis occurs during the process of tumor growth, invasion and metastasis, and is essential for the survival of solid tumors. As an integrin significantly overexpressed in human tumor vascular endothelial cells, $\alpha_v\beta_3$ is a suitable targeting site for anti-angiogenesis of tumor. We designed and prepared a self-assembling peptide (SAP) with the ability to targeting $\alpha_v\beta_3$ and self-assembly. SAP formed nanoparticles in solution and transformed into nanofibrous network once specifically binding to integrin $\alpha_v\beta_3$ on the surface of human umbilical vein endothelial cells (HUVECs). The SAP network stably anchored on HUVECs over 24 h, which consequently resulted in high-efficient inhibition of vascularization. *In vitro* anti-angiogenesis experiment displayed that the inhibition rate of tube-formation reached 94.9%. *In vivo* anti-angiogenesis array based on chick chorioallantoic membrane (CAM) model exhibited that the SAP had an inhibition rate up to 63.1%. These results indicated the outstanding anti-angiogenic ability of SAP, potentially for tumor therapy.

© 2020 Chinese Chemical Society and Institute of Materia Medica, Chinese Academy of Medical Sciences. Published by Elsevier B.V. All rights reserved.

Angiogenesis plays a key role in the growth and spread of malignant tumors by providing oxygen, nutrition and access to distant metastasis [1–4]. With gradually thorough mechanism research of tumor angiogenesis, abundant amount of anti-angiogenesis drugs has been developed [5–8]. Inhibition of angiogenesis as an adjuvant therapy for radiotherapy and chemotherapy has benefited many patients [9]. It is worth noting that the toxic side-effects of chemotherapy are relatively large and cannot be used without restriction [10–12]. In contrast, anti-angiogenic drugs are less toxic, so it can be taken continuously after chemotherapy, which is called maintenance therapy [13,14].

$\alpha_v\beta_3$ is one of the most studied member of integrin family. It exhibits abnormally high expression in tumor vascular endothelial cells and has become an important target for inhibiting tumor angiogenesis [9,15–17]. Upon binding to the vitronectin, integrin $\alpha_v\beta_3$ are activated into a high affinity state, which in turn leads to angiogenesis. Therefore, peptides or antibodies capable of targeting and interfering with the $\alpha_v\beta_3$-vitronectin interaction are classified as anti-angiogenic drugs [18,19]. Screened by high-throughput screening method, His-Ser-Asp-Val-His-Lys (HSDVHK) demonstrated acceptable ability to inhibit angiogenesis [20]. Due to the firm orthogonal docked orientation of HSDVHK at the interface between $\alpha_v$ and $\beta_3$ subunit, the binding constant of HSDVHK to integrin $\alpha_v\beta_3$ is twice that of the classical RGD sequence when binding to integrin $\alpha_v\beta_3$ [21]. However, targeting peptide monomers or nanoparticles tend to enter cells *via* endocytosis, resulting in decreased extracellular binding efficiency between ligand peptide, such as the binding between HSDVHK and integrin $\alpha_v\beta_3$ on cell surfaces. Inspired by the mechanism of dynamic self-assembly [22–26], attempts can be made to design self-assembling nano-material that is capable of intelligently deforming in specific physiological/pathological conditions, involving acidity, specific biomarkers and *etc.* [27–29]. In our previous works, for example, we designed a pH-responsive material that *in situ* self-assembled to form nest-like implants in tumor acidic environment for homing theranostic agents [30]. A dual-targeted (targeting integrin and laminin receptor) artificial extracellular matrix was also constructed to prevent the metastasis of breast and melanoma tumor [31]. In addition, an intelligent nanofibrous network capable of capturing vascular endothelial growth factor (VEGF) was designed to avoid the activating of vascular endothelial growth factor receptor (VEGFR), thus normalizing tumor vessels [32].

* Corresponding author.
*E-mail address:* wanglei@nanoctr.cn (L. Wang).

https://doi.org/10.1016/j.cclet.2020.04.006
1001-8417/© 2020 Chinese Chemical Society and Institute of Materia Medica, Chinese Academy of Medical Sciences. Published by Elsevier B.V. All rights reserved.

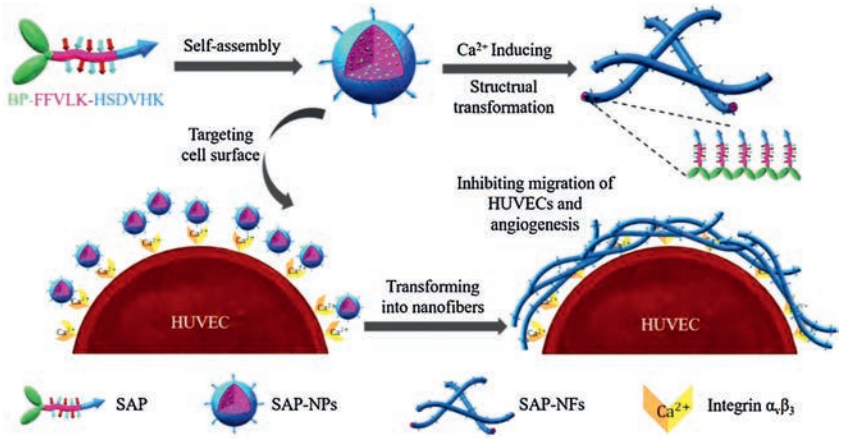


**Scheme 1.** Schematic illustration of $Ca^{2+}$ ions (simulating integrin $\alpha_v\beta_3$)-triggered (in solution) or integrin $\alpha_v\beta_3$-triggered (in cellular level) structural transformation from SAP nanoparticles (SAP-NPs) to nanofibers (SAP-NFs).

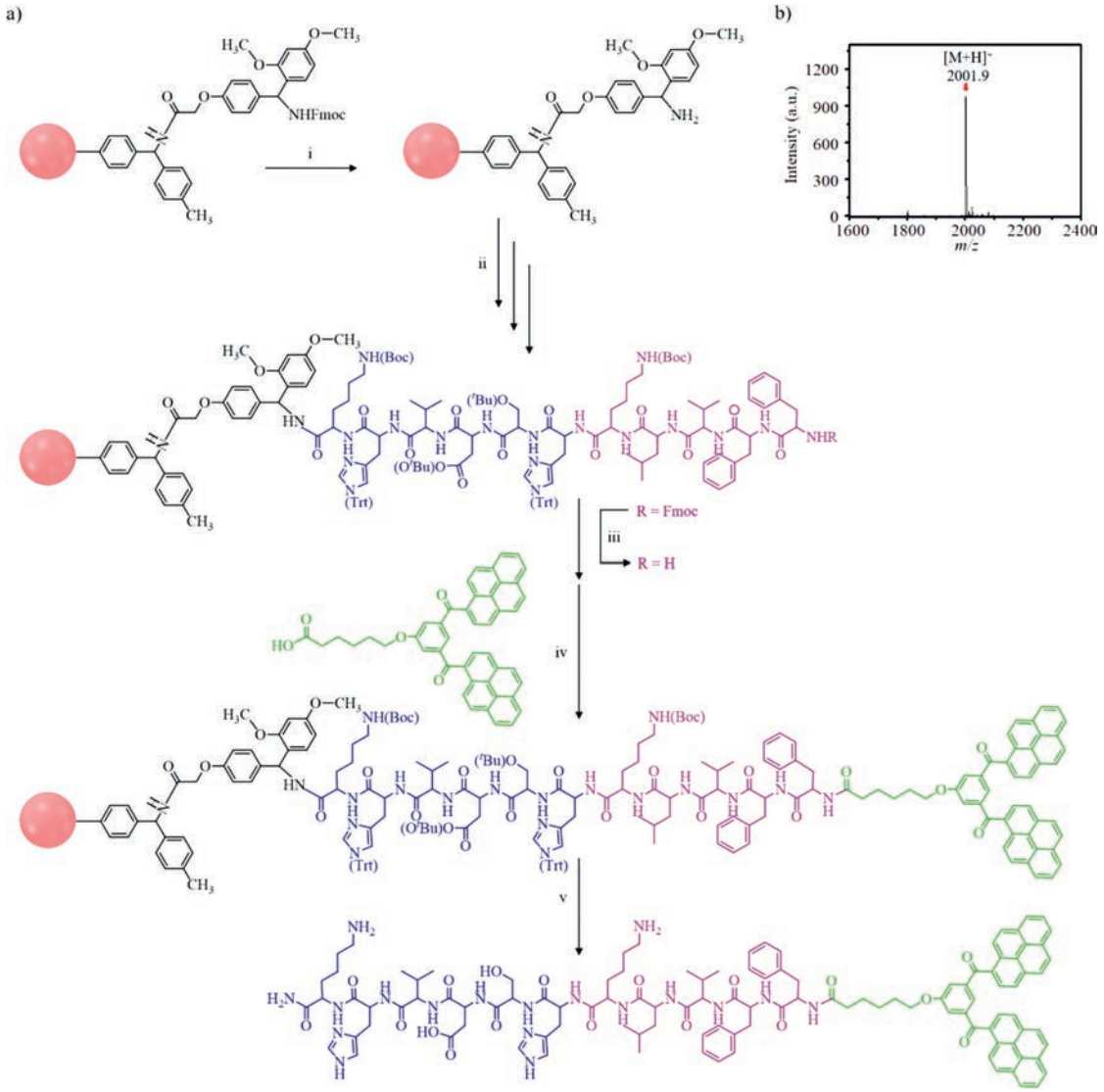


**Fig. 1.** (a) The synthetic route of SAP. (i) 20% piperidine in DMF, 15 min; (ii) Fmoc-based standard peptide solid phase synthesis method: Fmoc protected amino acids, HBTU, NMM, DMF, 1 h; (iii) 20% piperidine in DMF, 15 min; (iv) BP, HBTU, NMM, DMF, 6 h; (v) TFA/$H_2O$/TIS (95:2.5:2.5, v/v/v), 3 h. (b) The MALDI-TOF mass spectrum of SAP.

Herein, a self-assembling peptide (SAP), BP-FFVLK-HSDVHK, was successfully designed and synthesized as *in situ* constructible and enduring nanofibrous network for blocking the activity of endothelial cells and inhibiting angiogenesis. SAP consisted of three motifs: (i) an aromatic bis-pyrene (BP) motif as a strong hydrophobic core and fluorescence detection site [33], (ii) a FFVLK hydrogen-bonding peptide motif as a peptide-scaffold to form $\beta$-sheet nanofiber structures [34], (iii) a targeting HSDVHK peptide motif, as a ligand of integrin $\alpha_v\beta_3$, inducing structural transformation [20]. The SAP was rapidly injected into medium to obtain nanoparticles of SAP (SAP-NPs), and HUVECs were cultured in this medium system. Once binding with integrin $\alpha_v\beta_3$ receptor on the surface of HUVECs, SAP-NPs reassembled to form nanofibers (SAP-NFs) with a $\beta$-sheet structure and exhibited long-term retention (Scheme 1). At solution level, the structural transformation from SAP-NPs to SAP-NFs was distinctly confirmed by circular dichroism (CD), Fourier transform infrared spectroscopy (FT-IR) and transmission electron microscope (TEM). Furthermore, when co-incubated with HUVECs, similar morphological transformation was also observed by scanning electron microscope (SEM) and confocal laser scanning microscope (CLSM). Finally, the ability of angiogenesis inhibition was verified by tube-formation experiment and chick chorioallantoic membrane experiment. The SAP shows great potential of anti-angiogenesis for tumor therapy.

The SAP BP-FFVLK-HSDVHK was prepared by standard solid phase synthesis method from C to N terminal under Fmoc group protection system [22,35]. BP was attached to the peptide by amidation reaction before being cleaved from the resin (Fig. 1). As an aggregation-induced emission (AIE) molecule, the introducing of BP into peptides imparts similar AIE properties to SAP. The aggregation of SAP was explored by UV-vis absorption and fluorescence emission spectroscopy. Firstly, SAP solutions ($2.0 \times 10^{-5}$ mol/L) in $H_2O$/DMSO (dimethyl sulfoxide) solvent system with gradually increased $H_2O$ volume ratios (from 10% to 90%) were prepared through the method of rapid precipitation and tested by UV-vis absorption spectroscopy. The absorption band at 328-391 nm broadened and decreased significantly. Meanwhile, the bathochromic absorption peak increased slightly (Fig. 2a). In addition, the fluorescence emission of the SAP was significantly enhanced when the solvent system changed from pure DMSO to $H_2O$/DMSO, with maximum emissive peak at 515 nm (Fig. 2b), indicating the formation of BP aggregates [22,33].

With the strong hydrophobicity and large $\pi$-conjugation of BP motif, SAP was supposed to form nanoparticles (SAP-NPs), stabilized by the hydrophilic targeting peptide sequence HSDVHK. TEM characterization was performed to further explore morphology and size of the SAP-NPs, with a diameter of $239 \pm 72$ nm (Fig. 2c). In order to confirm the importance of $\beta$-sheet structured self-assembling sequence KLVFF, a control molecule BP-GGAAK-HSDVHK (C-SAP) was designed and prepared (Figs. S1 and S2 in Supporting information), which supposed to form nanoparticles without transformable ability. As expected, the C-SAP could self-assemble into C-SAP-NPs with similar diameter of $211 \pm 27$ nm (Fig. S3a in Supporting information).

There are three metal ion binding sites in the extracellular domain of the $\beta_3$ subunit of integrin $\alpha_v\beta_3$, among which the metal ion dependent adhesion site (MIDAS) can bind to $Ca^{2+}$ ions and further coordinate with the ligands [36]. Therefore, as a simplified model of integrin $\alpha_v\beta_3$, $Ca^{2+}$ ions were used to initially explore the morphology transformation of the nanoparticles [23]. The freshly prepared solution of SAP-NPs ($4.0 \times 10^{-5}$ mol/L, $H_2O$/DMSO (99:1, v/v)) were co-incubated with equal volume of $CaCl_2$ aqueous solution ($4.0 \times 10^{-5}$ mol/L). The morphological transformation of SAP-NPs was observed by TEM within 6 days (Fig. 2c). At the initial time point, $Ca^{2+}$ ion-induced SAP-NPs were spheres with a diameter of $145 \pm 47$ nm, which is smaller than that of SAP-NPs

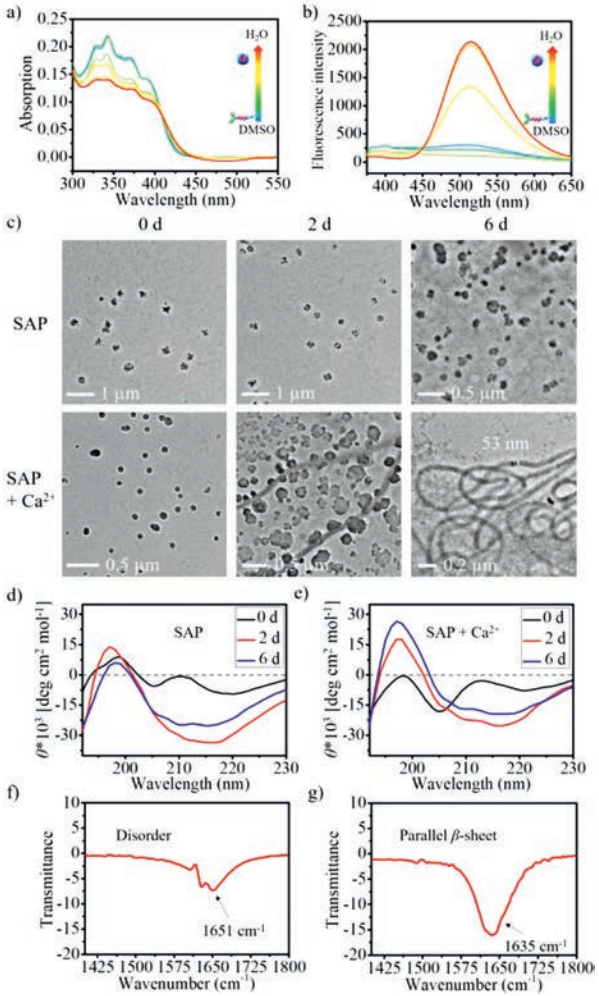


**Fig. 2.** Gradual change in UV-vis absorption (a) and fluorescence emission (b) of SAP when adding water into DMSO solution of SAP ($H_2O$:DMSO from 0:100, 10:90, 30:70, 50:50, 70:30 to 90:10 by volume ratio). (c) Corresponding TEM images showing the process of gradual morphology transformation with time. CD spectra of SAP nanoaggregates in the absence (d) or presence (e) of $Ca^{2+}$ ions in aqueous solution in 6 days. FT-IR characterization of SAP nanoaggregates in the presence of $Ca^{2+}$ ions in aqueous solution on day 0 (f) and day 6 (g).

without $Ca^{2+}$. It may be due to the fact that $Ca^{2+}$ ions compressed the electrostatic double layer [37]. On the second day, nanofibers were observed, accompanied by recombined SAP-NPs of non-uniform size. For day 6, uniform nanofibrous state was exhibited ($\Phi = 53 \pm 4$ nm), implying the structural transformation from SAP-NPs into SAP-NFs induced by $Ca^{2+}$. The SAP-NPs kept the particulate structures without $Ca^{2+}$ incubation. When incubating C-SAP-NPs with $Ca^{2+}$ ions under the same conditions, in contrast, it maintained particle state without morphological transformation (Fig. S3a), indicating the importance of hydrogen bond units (KLVFF) in the transformation process.

CD spectra were utilized to further illustrate the changes in the secondary structure of SAP during the transformation and the driving force of transformation. Incubating with $Ca^{2+}$ ions, SAP-NPs gradually formed a typical spectrum of $\beta$-sheet structure with a positive peak at 197 nm and a negative peak at 218 nm [38,39]. The increasing intensity of the peaks from day 2 to 6 probably indicated the formation of highly-ordered SAP-NFs with $\beta$-sheet ingredients (71.4% in day 6, Fig. 2e), which is much higher than that of SAP-NPs in the absence of $Ca^{2+}$ (32.5% in day 6, Fig. 2d). These results confirmed the necessity of $Ca^{2+}$ during morphological

transformation. The molecular packing mode in the $\beta$-sheet was further investigated by Fourier transform infrared (FT-IR) spectroscopy. The amide I region of FT-IR at 1651 $cm^{-1}$ (day 0, Fig. 2f) and 1635 $cm^{-1}$ (day 6, Fig. 2g) suggested the structure transition from random coil (SAP-NPs) to parallel $\beta$-sheet (SAP-NFs) [40]. In contrast, CD (Figs. S3b and S3c in Supporting information) and FT-IR (Figs. S3d and S3e in Supporting information) clearly demonstrated that C-SAP without morphological transformation ability maintained a random coil state throughout the experiment, regardless of whether $Ca^{2+}$ was provided. SAP and C-SAP formed nanoparticles in aqueous solution due to the strong hydrophobicity of BP. Moreover, SAP-NPs with morphological transformation ability self-assembled into nanofibers with parallel $\beta$-sheet structure under the induction of $Ca^{2+}$ ions.

In order to verify the targeting ability of SAP and the morphological transformation on the cell surface, HUVECs were selected, on which integrin $\alpha_v\beta_3$ are overexpressed. MCF-7 cells were used as a negative control. Cell viability was firstly defined by cell counting kit-8 (CCK-8) array to confirm the safe concentration of SAP and C-SAP on HUVECs (Fig. 3a) and MCF-7 (Fig. S4a in Supporting information). The results showed that cell killing rate of SAP ($IC_{50}$ = 155 μmol/L for HUVECs, 154 μmol/L for MCF-7) was similar to that of C-SAP ($IC_{50}$ = 139 μmol/L for HUVECs, 146 μmol/L for MCF-7) and had negligible cytotoxicity below $8.0 \times 10^{-5}$ mol/L. Therefore, a safe concentration of $2.0 \times 10^{-5}$ mol/L was selected as the standard condition for all cellular experiments, exhibiting that the biological effects of subsequent experiments are based on a non-killing mechanism.

The HUVECs were incubated with SAP-NPs or C-SAP-NPs for 4 h, respectively, and culture solutions were replaced by drug-free medium before observed by confocal laser scanning microscope (CLSM) and scanning electron microscope (SEM). SAP-NPs treated HUVECs exhibited green fluorescence on the surface, which may be due to the inhibition of internalization by *in situ* self-assembly from SAP-NPs to SAP-NFs after binding to integrin $\alpha_v\beta_3$ (Fig. 3b). Notably, green fluorescence intensity was still strong even after 24 h, indicating excellent retention of the SAP-NFs (Fig. S5 in Supporting information). HUVECs treated with C-SAP-NPs showed green fluorescence intracellularly, suggesting that nanoparticles were incorporated into the cells (Fig. 3c and Fig. S6 in Supporting information). SEM of the cell surface further supported this conclusion. Untreated HUVECs exhibited a smooth surface with slightly pleated protrusions. C-SAP-NPs treated group showed similar surface morphology except for some particles that could be non-internalized C-SAP-NPs. As expected, the SAP-NPs treated HUVECs were covered by a typical fibrous network, which could be transformed SAP-NFs (Fig. 3d), illustrating the critical role of hydrogen unit KLVFF in morphology transformation. In contrast, for MCF-7 cells with low expression of integrin $\alpha_v\beta_3$, only weak fluorescent signal can be detected (Figs. S4b and S4c in Supporting information) and the surface morphology after treatment with SAP-NPs or C-SAP-NPs were almost consistent with blank group (Fig. S4d in Supporting information), suggesting that ligand-receptor binding is a key factor in inducing morphology transformation and achieving long-term retention.

To evaluate the inhibition effect of SAP-NPs for migration and tube formation, a series of *in vitro* experiments were carried out, including wound healing, transwell-migration and tube-formation. Wound healing experiment was performed to test the inhibitory capacity of SAP and C-SAP. For highly active HUVECs, blank group cultured in drug-free medium were almost completely healed after being scratched for 36 h (Fig. 4a). Wound healing rate of the blank group was defined as 100%, and the healing rate of the SAP group was 23.9%, which was much lower than that (38.2%) of the C-SAP group (Fig. 4b). Migration experiments based on transwell chambers were performed to further verify the inhibition of the SAP-NPs and C-SAP-NPs (Fig. 4c). HUVECs were

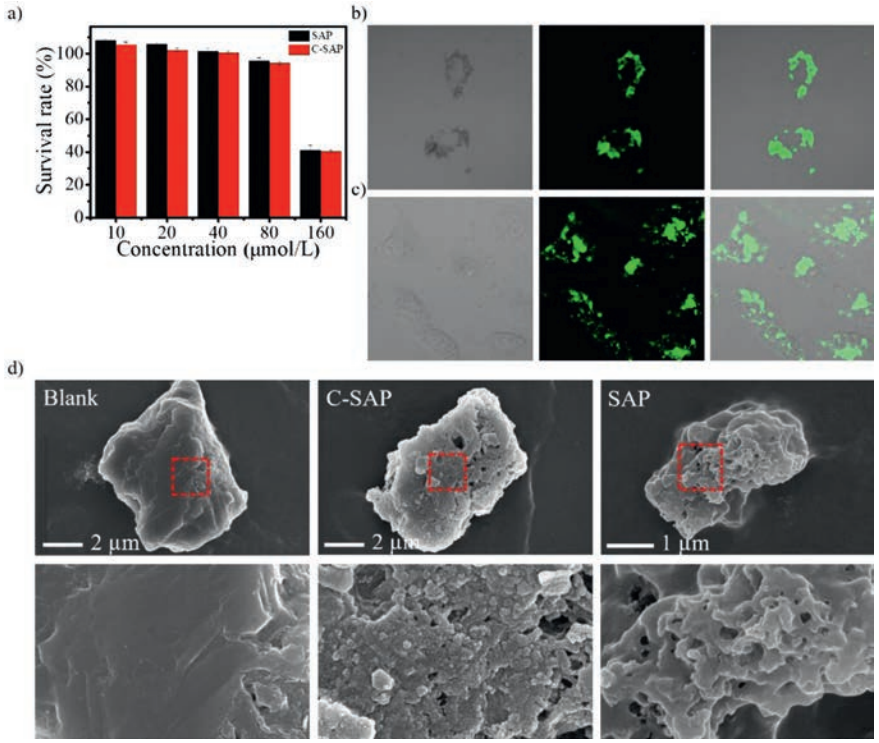


**Fig. 3.** (a) Cell viability of HUVECs treated with SAP-NPs or C-SAP-NPs by CCK-8 array. CLSM images of HUVECs incubated with SAP-NPs (b) and C-SAP-NPs (c) for 4 h. (d) SEM images of cell surface of HUVECs treated with SAP-NPs or C-SAP-NPs, untreated HUVECs served as a blank control.

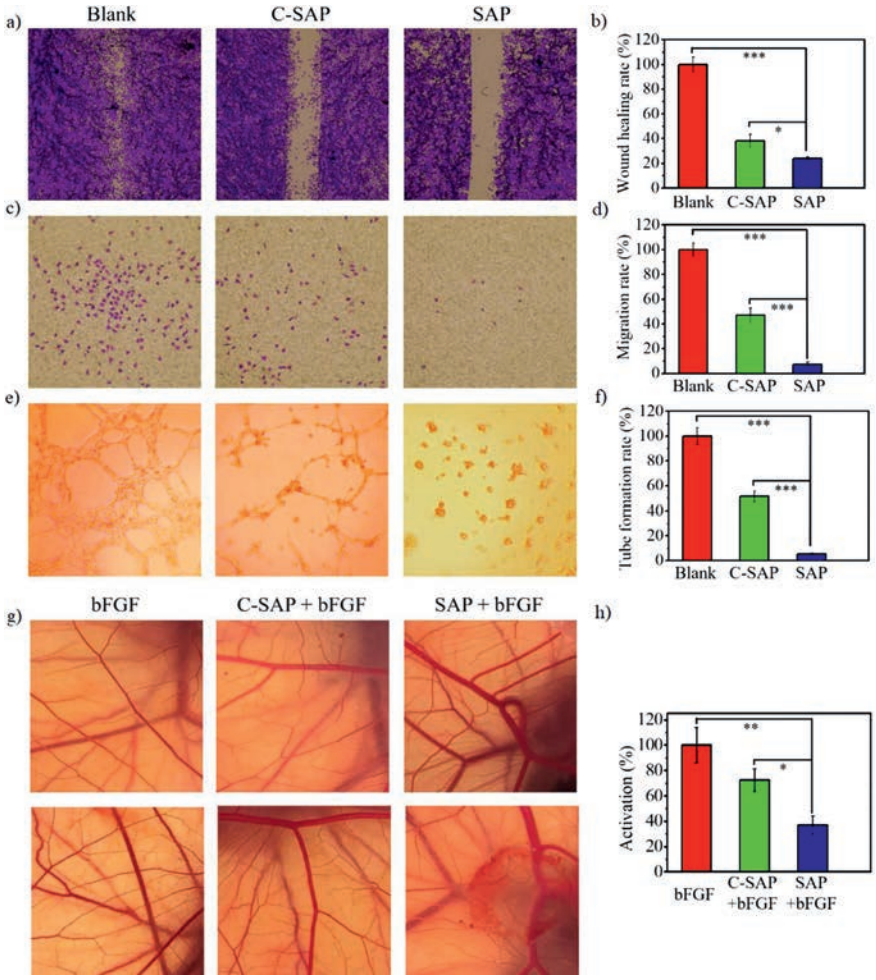


**Fig. 4.** Microscopy images of wound healing (a), cell migration (c), tube-formation (e) and statistical quantitative analysis (b, d, f) of HUVECs. The untreated first group served as a blank control group. The second and third groups were incubated with C-SAP-NPs and SAP-NPs for 36 h, respectively. (g) Microscopy images of chick chorioallantoic membrane and corresponding (h) statistical quantification results. The chicken embryo was nine days old at the start of the experiment. The increment of the number of blood vessels is adopted as the basis for evaluation. Data were given in the form of mean ± SD ($n = 3$). $^{*}P < 0.05$, $^{**}P < 0.01$, $^{***}P < 0.001$.

cultured in a nutrient-deficient upper chamber, separated from nutrient-rich medium by a layer of porous polycarbonate membrane. SAP-NPs and C-SAP-NPs inhibited the longitudinal motility ability of HUVECs by 92.7% and 53.1%, respectively (Fig. 4d), demonstrating the satisfactory inhibition ability of SAP. For MCF-7 cells with weak migration ability and low expression of integrin $\alpha_v\beta_3$, neither C-SAP-NPs nor SAP-NPs had significant effects on migration of cells (Fig. S7 in Supporting information).

Matrigel provides a biologically active environment similar to the mammalian cell basement membrane, in which HUVECs are stimulated to form tubes [41]. HUVECs were incubated with C-SAP-NPs or SAP-NPs for 9 h in the presence of matrigel to verify the ability of the samples to inhibit tube-formation (Fig. 4e). It was observed that the untreated HUVECs form an abundant and dense tubular network, while C-SAP-NPs treated group presented sparse tubes with an inhibition rate of 48.7%. Surprisingly, SAP-NPs almost completely inhibited tube-formation, exhibiting an inhibition rate up to 94.9% (Fig. 4f). HUVECs formed cell clusters and were not linked to each other, proving the excellent anti-angiogenic potential of SAP with targeting and *in situ* self-assembling capability.

To discuss the anti-angiogenesis effect by SAP and C-SAP *in vivo*, a basic FGF (bFGF)-induced CAM assay was employed [20]. The chicken embryos were nine days old at the start of the experiment. To the CAM surfaces, 10 ng bFGF and 10 μg SAP or C-SAP dissolved in 50 μL physiological saline were added, and the eggs were incubated at 37 °C for 2 days. CAMs were observed and photographed before and after incubation (Fig. 4g). The increment of the number of blood vessels was adopted as the basis for evaluating efficacy of anti-angiogenesis. SAP-NPs inhibited angiogenesis with a satisfactory inhibition rate of 63.1% compared to bFGF control group, whereas C-SAP-NPs appeared to have a weak inhibition rate of 27.1% (Fig. 4h).

In conclusion, self-assembly of peptides, as a flexible strategy, have the advantages of precise controllability, excellent biocompatibility and *etc*. We developed an accurate strategy to construct ligand nano-network for inhibition of angiogenesis. The SAP monomers formed SAP-NPs due to hydrophilic and hydrophobic interaction dominated by BP, and self-assembled to form SAP-NFs once the ligand targeting to integrin $\alpha_v\beta_3$. The ligand nano-network avoid being degraded by endocytosis of cells and could block the motility and migration of HUVECs, thereby inhibiting angiogenesis. This strategy of *in situ* construction nano-network shows great potential as an anti-angiogenic drug for adjuvant therapy against tumors.

## Declaration of competing interest

The authors declare that they have no known competing financial interests or personal relationships that could have appeared to influence the work reported in this paper.

## Acknowledgments

This work was supported by the National Natural Science Foundation of China (Nos. 51890891,51725302, 21807020, 51573031 and 51573032), Science Fund for Creative Research Groups of the National Natural Science Foundation of China (No. 11621505), CAS Interdisciplinary Innovation Team, Jilin Province Key Laboratory of Organic Functional Molecular Design and Synthesis (No. 130028911) and Key Laboratory of Biomedical Effects of Nanomaterials and Nanosafety, CAS (No. NSKF201807).

## Appendix A. Supplementary data

Supplementary material related to this article can be found, in the online version, at doi:https://doi.org/10.1016/j.cclet.2020.04.006.

## References

[1] P. Carmeliet, R.K. Jain, Nature 407 (2000) 249–257.
[2] J. Folkman, Nat. Med. 1 (1995) 27–30.
[3] D. Hanahan, R.A. Weinberg, Cell 144 (2011) 646–674.
[4] M. de Palma, D. Biziato, T.V. Petrova, Nat. Rev. Cancer 17 (2017) 457–474.
[5] C.L. Chaffer, R.A. Weinberg, Science 331 (2011) 1559–1564.
[6] A.R. Reynolds, I.R. Hart, A.R. Watson, et al., Nat. Med. 15 (2009) 392–400.
[7] L.J. van't Veer, H. Dai, M.J. van de Vijver, et al., Nature 415 (2002) 530–536.
[8] D.F. McDermott, M.A. Huseni, M.B. Atkins, et al., Nat. Med. 24 (2018) 749–757.
[9] P. Carmeliet, R.K. Jain, Nature 473 (2011) 298–307.
[10] M. Dean, T. Fojo, S. Bates, Nat. Rev. Cancer 5 (2005) 275–284.
[11] P. Horcajada, T. Chalati, C. Serre, et al., Nat. Mater. 9 (2010) 172–178.
[12] P. van Hagen, M.C.C.M. Hulshof, J.J.B. van Lanschot, et al., N. Engl. J. Med. 366 (2012) 2074–2084.
[13] M. Guba, P. von Breitenbuch, M. Steinbauer, et al., Nat. Med. 8 (2002) 128–135.
[14] J. Folkman, Exp. Cell Res. 312 (2006) 594–607.
[15] J.S. Desgrosellier, D.A. Cheresh, Nat. Rev. Cancer 10 (2010) 9–22.
[16] F. Zhao, L. Li, L. Guan, et al., Cancer Lett. 344 (2014) 62–73.
[17] B.P. Gray, K.C. Brown, Chem. Rev. 114 (2014) 1020–1081.
[18] P.C. Brooks, S. Strömblad, R. Klemke, et al., J. Clin. Invest. 96 (1995) 1815–1822.
[19] E. Ruoslahti, Cancer Cell 2 (2002) 97–98.
[20] Y. Lee, D.K. Kang, S.I. Chang, et al., J. Biomol, Screen 9 (2004) 687–694.
[21] Y. Choi, E. Kim, Y. Lee, et al., Proteomics 10 (2010) 72–80.
[22] P.P. Yang, X.X. Zhao, A.P. Xu, et al., J. Mater. Chem. B 4 (2016) 2662–2668.
[23] A.P. Xu, P.P. Yang, C. Yang, et al., Nanoscale 8 (2016) 14078–14083.
[24] X. Liang, L. Wang, K. Jeong, et al., Chin. Chem. Lett. 30 (2019) 123–126.
[25] P. Yang, C. Yang, K. Zhang, et al., Chin. Chem. Lett. 29 (2018) 1811–1814.
[26] X. Guo, X. Wei, Z. Chen, et al., Pro. Mater. Sci. 107 (2020) 100599.
[27] P.P. He, X.D. Li, L. Wang, et al., Acc. Chem. Res. 52 (2019) 367–378.
[28] D.B. Cheng, X.H. Zhang, Y.J. Gao, et al., J. Am. Chem. Soc. 141 (2019) 7235–7239.
[29] H.W. An, L.L. Li, Y. Wang, et al., Nat. Commun. 10 (2019) 4861.
[30] P.P. Yang, Q. Luo, G.B. Qi, et al., Adv. Mater. 29 (2017) 1605869.
[31] X.X. Hu, P.P. He, G.B. Qi, et al., ACS Nano 11 (2017) 4086–4096.
[32] B.N. Li, P.P. He, P.P. Yang, et al., J. Mater. Chem. B 6 (2018) 5282–5289.
[33] L. Wang, W. Li, J. Lu, et al., J. Phys. Chem. C 117 (2013) 26811–26820.
[34] S. Pellegrino, N. Tonali, E. Erba, et al., Chem. Sci. 8 (2017) 1295–1302.
[35] G.B. Fields, R.L. Noble, Int. J. Pept. Protein Res. 35 (1990) 161–214.
[36] J.F. Van Agthoven, J.P. Xiong, J.L. Alonso, et al., Nat. Struct. Mol. Biol. 21 (2014) 383–388.
[37] V. Pavet, J. Beyrath, C. Pardin, et al., Cancer Res. 70 (2010) 1101–1110.
[38] S.N. Nguyen, C.E. Bobst, I.A. Kaltashov, Mol. Pharm. 10 (2013) 1998–2007.
[39] N.M. Pinkerton, A. Grandeury, A. Fisch, et al., Mol. Pharm. 10 (2013) 319–328.
[40] N. Lorenzen, S.B. Nielsen, A.K. Buell, et al., J. Am. Chem. Soc. 136 (2014) 3859–3868.
[41] D. Lyden, K. Hattori, S. Dias, et al., Nat. Med. 7 (2001) 1194–1201.